

NUMERICAL STUDY OF THE EFFECTS OF LARGE BLOOD VESSELS ON THREE-DIMENSIONAL TISSUE TEMPERATURE PROFILES DURING CRYOSURGERY

Zhong-Shan Deng and Jing Liu

*Cryogenics Laboratory, Technical Institute of Physics and Chemistry,
Chinese Academy of Sciences, Beijing, China*

Large blood vessels can produce steep temperature gradients in frozen tissues, resulting in inadequate cooling temperatures during cryosurgery. In addition, blocking of blood vessels and/or bleeding due to ruptures of large blood vessels by the iceball during the cryoablation procedure may cause undesired damage to healthy tissues or organs. However, such important issues have received little attention up to now. In this article, several typical vascular models, which have been widely used in simulation of tissue temperature during tumor hyperthermia, are applied to study the effects of large blood vessels on the transient tissue temperature distributions during cryosurgery treatment. The thermal model combines the Pennes bioheat transfer equation describing perfused tissues and the energy equation for single or countercurrent large blood vessels with a constant Nusselt number. A finite-difference algorithm based on the effective heat capacity method is applied to solve these complex heat transfer problems with phase change in biological tissues embedded with large blood vessels. In the algorithm, the tissues are treated as nonideal materials, freezing over a temperature range, and the effects of blood perfusion and metabolic heat generation in the unfrozen tissues are also included. Numerical analyses are then performed to test the influence of the blood vessels on the temperature distributions of tissues. The results indicate that different vascular models produce significantly different temperature transients for a given freezing pattern. Therefore, without careful treatment planning on some specific tumors close to or with large vessels transmitting through, the final cryosurgery may turn out to fail. In other words, insufficient cooling of the targets due to heating of large and warm blood vessels may lead to the regeneration of tumor cells. This study has raised quite a few important issues in modeling the cryosurgical phase-change behavior of living tissues embedded with large blood vessels.

INTRODUCTION

Cryosurgery, sometimes referred to as cryotherapy or cryoablation, is a form of treatment performed with an instrument that freezes and destroys the diseased tissue, and is fast becoming a minimally invasive surgical technique. One of the biggest breakthroughs in the field of cryosurgery for tumor treatment has been the application of intraoperative ultrasound to monitor the cryosurgical destruction

Received 13 December 2004; accepted 11 June 2005.

This work was partially supported by the National Natural Science Foundation of China under Grants 50325622 and 50436030.

Address correspondence to Jing Liu, Cryogenics Laboratory, P.O. Box 2711, Technical Institute of Physics and Chemistry, Chinese Academy of Sciences, Beijing 100080, China. E-mail: jliu@cl.cryo.ac.cn

NOMENCLATURE

<p>C heat capacity, $\text{J}/\text{m}^3\text{ }^\circ\text{C}$</p> <p>$D$ diameter of vessel, m</p> <p>$\text{Fo} = (\tilde{k} \Delta t)/(\tilde{C} \Delta x^2)$</p> <p>$h$ convective heat transfer coefficient, $\text{W}/\text{m}^2\text{ }^\circ\text{C}$</p> <p>$k$ thermal conductivity, $\text{W}/\text{m }^\circ\text{C}$</p> <p>$\text{Nu}$ Nusselt number</p> <p>P perimeter of vessel, m</p> <p>Q_l latent heat, J/m^3</p> <p>Q_m metabolic heat generation, W/m^3</p> <p>R thermal resistance, $\text{m }^\circ\text{C}/\text{W}$</p> <p>$S$ cross-sectional area of vessel, m^2</p> <p>t time, s</p> <p>T temperature, $^\circ\text{C}$</p> <p>T_a artery temperature, $^\circ\text{C}$</p> <p>T_m freezing point of ideal tissue, $^\circ\text{C}$</p> <p>T_{ml} lower phase transition temperature of tissue, $^\circ\text{C}$</p> <p>T_{mu} upper phase transition temperature of tissue, $^\circ\text{C}$</p> <p>T_w temperature at probe tip, $^\circ\text{C}$</p>	<p>T_{wb} temperature of the vessel wall, $^\circ\text{C}$</p> <p>v velocity of blood flow, m/s</p> <p>$W = \tilde{\omega}_b C_b / \tilde{C}$</p> <p>$x, y, z$ Cartesian coordinate, m</p> <p>\mathbf{X} location</p> <p>β parameter taking a value between 0 and 1</p> <p>Δ step size</p> <p>π circular constant</p> <p>ω_b blood perfusion, $\text{ml}/\text{s}/\text{ml}$</p> <p>$\Omega$ computation domain</p> <p>Subscripts</p> <p>b blood</p> <p>f frozen tissue</p> <p>t tumor</p> <p>u unfrozen tissue</p> <p>0 initial value</p> <p>Superscript</p> <p>\sim effective value</p>
---	---

process. Under the monitoring of ultrasound, the size of the iceball created during the cryosurgery procedure can be carefully controlled, and complete ablation of the undesirable tissues is then assured. Generally speaking, cryosurgery has the advantage of being an excellent technique that spares much more noncancerous tissue than conventional surgical resection [1].

As is well known, tumor growth and survival ultimately depends critically on its blood vessel network. The process of neovascularization, as shown in Figure 1, is a universal characteristic of solid cancers larger than a few millimeters [2], which results from the fact that tumors are often situated near some large blood vessels. In addition, some malignancies, such as pancreatic tumors, encase the aorta and other major vessels (as shown in Figure 2) [3]. The presence of tumor involvement of vessels will, in most cases, make the patient ineligible for curative resection. Therefore the use of cryosurgery in these cases often appears as an attractive choice. However, it can be a plague to implement cryosurgery when a tumor is too close to a critical blood vessel or such vessel transits the tumor. There are two main reasons for this: on the one hand, the heating nature of the flowing blood in the large vessels can produce steep temperature gradients in frozen tissues, resulting in inadequate cooling temperatures and then contributing to nonkilling of tumor during cryosurgery; on the other hand, cutting off circulation of blood vessels and/or bleeding due to rupture of large blood vessels by the iceball during the cryoablation procedure may cause undesired damage to healthy tissues [4]. In addition, there is still much concern about the effect of cryotherapy on major vessels in a young patient with anticipated subsequent growth [5], although blood vessels do seem to tolerate some freezing [6]. In order to implement effective cryosurgery for the case of large blood

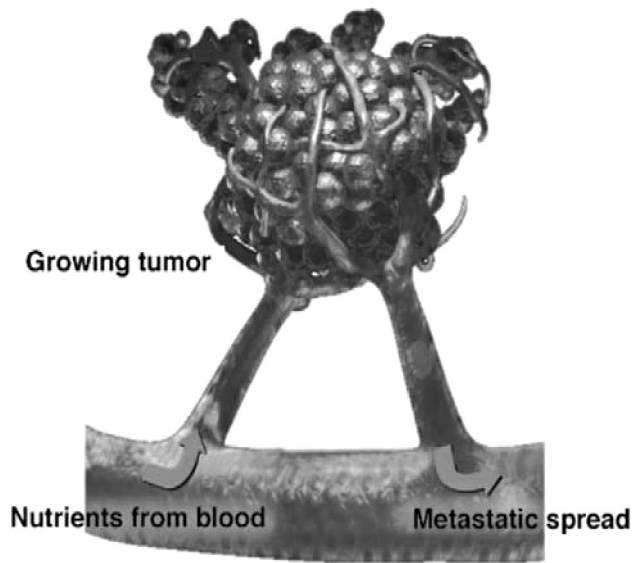


Figure 1. Tumor blood vessel network [2] (citation with permission).

vessels embedded in or close to the tumor, the effects of large blood vessels on the transient temperature distributions of tissues subject to controlled freezing must be well understood. Unfortunately, the current situation is that little is known about the role of the large blood vessels in the freezing behavior of living tissues, and most



Figure 2. Angiography for pancreatic cancer [3]. Coronal three-dimensional volume-rendered multidetector computed tomography (CT) scan shows pancreatic tumor (arrows) encasing mid-portion of superior mesenteric artery (arrowhead). This tumor was not eligible for curative resection (citation with permission).

of the existing studies [7–14] on the freezing behavior of living tissues during cryosurgery have been based on the classical bioheat transfer model—the Pennes bioheat equation, in which a collective perfusion term is used to reflect the thermal effect of blood flow. However, the Pennes equation has the inherent limitation that it cannot simulate the effects of widely spaced thermally significant blood vessels [15]. Such vessels are distributed throughout the body, and can perturb the temperature field of tissue [16]. In particular, when large blood vessels are present, the convective effect of the blood flow may significantly heat the surrounding cold tissues frozen by the cryoprobe, thus possibly forming steep temperature gradients between large blood vessels and the tissues near the vessels. If such temperature gradients are present, the freezing protocol must be revised to provide adequate freezing and to avoid damaging normal tissue. As is well known, any revision of the freezing protocol depends on the tissue temperature responses to it. Therefore, a quantitative mathematical model including the thermal effects of large blood vessels is urgently needed for predicting the temperatures of tissues subject to freezing.

Many vascular heat transfer models currently exist which account for the convective effects of large blood vessels on the temperatures of tissues. However, most of them were developed for hyperthermia [17–29] or for basic bioheat studies [15, 30–45], and did not take into consideration the cryosurgical phase-change heat transfer in living tissues with large blood vessels. Among them, Chato's work [30] was among the first to investigate the thermal behaviors of blood vessels. By introducing several simplifications, he solved analytically the temperature fields for a single vessel and a countercurrent vessel pair embedded in nonperfused tissues. Weinbaum-Jiji's modified bioheat transfer equation [31], which did not explicitly include large blood vessels, is also used as an alternative equation to study bioheat transfer problems. Lagendijk and his colleagues established a discrete vasculature thermal model, in which the vessel network is described as a structured tree of vessel segments [40, 42]. Chen and Roemer [20] developed several vascular models, and then studied the effects of large blood vessels on the tissue temperature distributions during simulated hyperthermia. Due to its important applications in tumor hyperthermia, the study of thermal behavior of large blood vessels has been a focus in the bioheat transfer field. Unfortunately, little attention has been paid to the effects of large blood vessels on the phase-change heat transfer in living tissues subject to freezing. Quite recently, Zhang et al. [4] made the first attempt to develop a theoretical model as well as simulating experiments for cryogenic heat transfer in biological tissues embedded with large blood vessels. They proposed a conceptual model for characterizing the heat transfer in two-dimensional cylindrical tissues with a single blood vessel, and solved it analytically. Using this model, they investigated the influence of the blood vessel entrance temperature, the vessel diameter, the blood flow velocity, and the vessel length on the tissue temperature distributions. However, due to the complexity of such problems, only a two-dimensional steady-state case with a single blood vessel transiting the tissues was considered. The details of three-dimensional transient cases with a single vessel or a countercurrent vessel pair, which is more real, are still unknown. Tremendous efforts are needed to probe into such important issues.

In this study, several typical vascular models, which have been widely used in hyperthermia modeling, are applied to study the effects of large blood vessels on the tissue temperature distributions during cryosurgery. Both the convective mechanism

of blood flow in the large blood vessels and the heat source mechanism of the perfused blood are considered. Due to the complexity, the models are solved by a numerical algorithm based on the effective heat capacity method. The numerical solutions are then used to demonstrate the influence of the different vessel models on tissue temperature fields during cryosurgery. The present work is expected to be valuable in optimizing cryosurgery procedures in which the tissues are embedded with large blood vessels.

MODELS AND ALGORITHM DEVELOPMENT

In this study, four different vascular models with typical geometric configurations are applied to simulate the cryogenic heat transfer of *in situ* tissues (shown in Figure 3), which include: (1) the bioheat transfer equation model, BHTE; (2) a model with a single artery transiting the tumor, SATT; (3) a model with a single artery close to the tumor, SACT; and (4) a model with countercurrent-flow vessels close to the tumor, CVCT. The boundary conditions are a constant temperature of 37°C on all surfaces of the parallelepiped. Similar vascular models were first developed to study the effects of large blood vessels on temperature distributions during simulated hyperthermia by Chen and Roemer [20]. In these models, the whole tissue domain consists of unfrozen tissue, frozen tissue, and large blood vessel domains.

In order to avoid the time-consuming iteration at the moving boundary, the effective heat capacity method is used in this study. A detailed description of the effective heat capacity method for the BHTE model (shown in Figure 3a) has been presented in our previous study [46]. The derivation is not repeated here, for brevity. In this study, the tissues are treated as nonideal materials, freezing over a temperature range (T_{ml} , T_{mu}), where T_{ml} and T_{mu} are respectively the lower and upper phase transition temperatures of tissue, aiming to reflect a relatively real clinical situation. Then the uniform energy equation for the unfrozen and frozen biological tissues can be written as

$$\tilde{C} \frac{\partial T}{\partial t} = \nabla \cdot \tilde{k} \nabla T - \tilde{\omega}_b C_b T + \tilde{Q}_m + \tilde{\omega}_b C_b T_a \quad \mathbf{X} \in \Omega \quad (1)$$

where C_b is the heat capacity of blood; \mathbf{X} contains the Cartesian coordinates x , y , and z ; Ω denotes the analyzed domain; T the tissue temperature; T_a the arterial temperature; \tilde{C} the effective heat capacity; \tilde{k} the effective thermal conductivity; \tilde{Q}_m the effective metabolic heat generation; $\tilde{\omega}_b(T)$ the effective blood perfusion; and

$$\tilde{C}(T) = \begin{cases} C_f & T < T_{ml} \\ \frac{Q_l}{(T_{mu} - T_{ml})} + \frac{C_f + C_u}{2} & T_{ml} \leq T \leq T_{mu} \\ C_u & T > T_{mu} \end{cases} \quad (2)$$

$$\tilde{k}(T) = \begin{cases} k_f & T < T_{ml} \\ \frac{(k_f + k_u)}{2} & T_{ml} \leq T \leq T_{mu} \\ k_u & T > T_{mu} \end{cases} \quad (3)$$

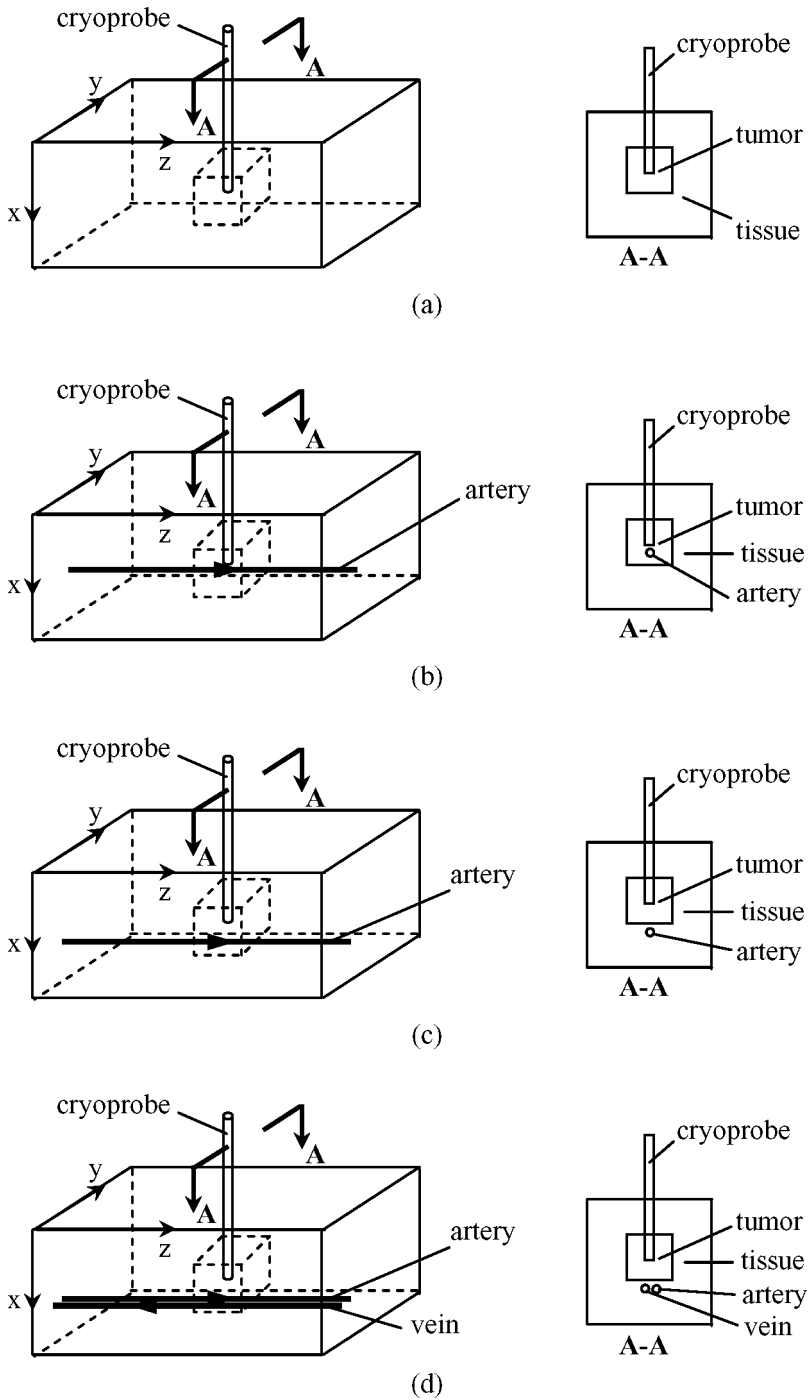


Figure 3. Illustration of several typical vascular models: (a) bioheat transfer equation model, BHTE; (b) a model with a single artery transiting the tumor, SATT; (c) a model with a single artery close to the tumor, SACT; (d) a model with countercurrent flow vessels close to the tumor, CVCT.

$$\tilde{Q}_m(T) = \begin{cases} 0 & T < T_{ml} \\ 0 & T_{ml} \leq T \leq T_{mu} \\ Q_m & T > T_{mu} \end{cases} \quad (4)$$

$$\tilde{\omega}_b(T) = \begin{cases} 0 & T < T_{ml} \\ 0 & T_{ml} \leq T \leq T_{mu} \\ \omega_b & T > T_{mu} \end{cases} \quad (5)$$

where C_u, C_f are, respectively, the heat capacity of unfrozen and frozen tissues; Q_l is the latent heat of tissue; k_u, k_f are the thermal conductivity of unfrozen and frozen tissues; ω_b is the blood perfusion of unfrozen tissue; and Q_m is the metabolic heat generation of unfrozen tissue. For simplicity, \tilde{C} in Eq. (2) and \tilde{k} in Eq. (3) are taken as constant when $T_{ml} \leq T \leq T_{mu}$.

Additionally, in these models the temperature of blood in large vessels, which varies along the flow direction, is governed by the convective heat transfer equation

$$C_b \frac{\partial T_b}{\partial t} = \frac{hP}{S} (T_{wb} - T_b) - C_b v \frac{\partial T_b}{\partial z} \quad (6)$$

where $h = \text{Nu} \cdot k_b / D$ is the convective heat transfer coefficient between the blood and tissue, D is the diameter of the vessel, P is the perimeter of the vessel, S is the cross-sectional area of the vessel, v the mean blood velocity along the vessel, Nu the Nusselt number, and T_{wb} the wall temperature of the vessel. Similar to the study of Chato [30], conduction inside the vessel in the z direction (flow direction) is neglected for large flow rate, and a constant Nusselt number is assumed. The sign of blood velocity v is assigned as positive, i.e., the velocities for bloods in artery and vein are positive and minus, respectively.

Applying the explicit finite-difference formulation to Eq. (1) and using the following relation to express the linear term T on the right side of Eq. (1),

$$T(\mathbf{X}, t) = \beta T(\mathbf{X}, t + \Delta t) + (1 - \beta) T(\mathbf{X}, t) \quad (7)$$

where β is a relaxation factor and $0 \leq \beta \leq 1$. Equation (5) can be discretized as

$$\begin{aligned} T(\mathbf{X}, t + \Delta t) = & \frac{1 - W(1 - \beta)\Delta t - m \cdot \text{Fo}}{1 + W\beta\Delta t} T(\mathbf{X}, t) + \sum_{i=1}^{m/2} \frac{\text{Fo}}{1 + W\beta\Delta t} T(\mathbf{X} + \Delta\mathbf{X}_i, t) \\ & + \sum_{i=1}^{m/2} \frac{\text{Fo}}{1 + W\beta\Delta t} T(\mathbf{X} - \Delta\mathbf{X}_i, t) + \frac{[\tilde{Q}_m + \tilde{\omega}_b C_b T_a] \Delta t}{1 + W\beta\Delta t} \end{aligned} \quad (8)$$

where Δt is the time increment; $W = \tilde{\omega}_b C_b / \tilde{C}$, and $\text{Fo} = (\tilde{k} \cdot \Delta t) / (\tilde{C} \cdot \Delta x^2)$ is the Fourier number; $m = 2, 4, 6$ correspond to the cases of one, two, and three dimensions, respectively; $\Delta\mathbf{X}_1 = (\Delta x, 0, 0)$, $\Delta\mathbf{X}_2 = (0, \Delta y, 0)$, $\Delta\mathbf{X}_3 = (0, 0, \Delta z)$.

For the vascular models, the finite-difference formulation in the blood vessel domain needs special treatment. In order to avoid the convective numerical instabilities, the upwind scheme is used to discretize the convective term in Eq. (6). Referring

to the formulation presented in [20], the general finite-difference equation for the different types of vessels can be written as

$$C_b \frac{T_{i,j,k}^{n+1} - T_{i,j,k}^n}{\Delta t} = \frac{T_{i+1,j,k}^{n+1} - T_{i,j,k}^{n+1}}{S \cdot R_{i+1/2}} - \frac{T_{i,j,k}^{n+1} - T_{i-1,j,k}^{n+1}}{S \cdot R_{i-1/2}} + \frac{T_{i,j+1,k}^{n+1} - T_{i,j,k}^{n+1}}{S \cdot R_{j+1/2}} - \frac{T_{i,j,k}^{n+1} - T_{i,j-1,k}^{n+1}}{S \cdot R_{j-1/2}} - C_b v \frac{T_{i,j,k}^{n+1} - T_{i,j,k-1}^{n+1}}{\Delta z} \quad (9)$$

The subscripted R 's are the thermal resistance between the center vessel node (i, j, k) and the four neighboring tissue nodes outside the vessel. These thermal resistances are composed of two parts, the convective and conductive resistances. The total thermal resistances between the two nodes, (i, j, k) and $(i-1, j, k)$, (i, j, k) and $(i+1, j, k)$, (i, j, k) and $(i, j-1, k)$, (i, j, k) and $(i, j+1, k)$, are, respectively [20],

$$R_{i-1/2} = R_{i+1/2} = \frac{4}{h\pi D} + \frac{2}{\pi k} \ln \frac{\Delta x}{D/2} \quad (10)$$

$$R_{j-1/2} = R_{j+1/2} = \frac{4}{h\pi D} + \frac{2}{\pi k} \ln \frac{\Delta y}{D/2} \quad (11)$$

where D is the diameter of the vessel. For countercurrent vessel pairs, the thermal resistance between the artery and the vein is

$$R_{a-v} = \frac{8}{h\pi D} + \frac{4}{\pi k} \ln \frac{\Delta y}{D} \quad (12)$$

For the four neighboring tissue nodes outside the vessel, the finite-difference formulations are different from those for the other tissue nodes, and are, respectively,

$$\begin{aligned} \tilde{C} \frac{T_{i-1,j,k}^{n+1} - T_{i-1,j,k}^n}{\Delta t} &= \frac{T_{i,j,k}^{n+1} - T_{i-1,j,k}^{n+1}}{S \cdot R_{i-1/2}} + \frac{\tilde{k} (T_{i-2,j,k}^{n+1} - T_{i-1,j,k}^{n+1})}{\Delta x^2} \\ &+ \tilde{k} \left(\frac{T_{i-1,j+1,k}^{n+1} - 2T_{i-1,j,k}^{n+1} + T_{i-1,j-1,k}^{n+1}}{\Delta y^2} + \frac{T_{i-1,j,k+1}^{n+1} - 2T_{i-1,j,k}^{n+1} + T_{i-1,j,k-1}^{n+1}}{\Delta z^2} \right) \\ &- \tilde{\omega}_b C_b \left[\beta T_{i-1,j,k}^{n+1} + (1 - \beta) T_{i-1,j,k}^n \right] + \tilde{Q}_m + \tilde{\omega}_b C_b T_a \end{aligned} \quad (13)$$

$$\begin{aligned} \tilde{C} \frac{T_{i+1,j,k}^{n+1} - T_{i+1,j,k}^n}{\Delta t} &= \frac{T_{i,j,k}^{n+1} - T_{i+1,j,k}^{n+1}}{S \cdot R_{i+1/2}} + \frac{\tilde{k} (T_{i+2,j,k}^{n+1} - T_{i+1,j,k}^{n+1})}{\Delta x^2} \\ &+ \tilde{k} \left(\frac{T_{i+1,j+1,k}^{n+1} - 2T_{i+1,j,k}^{n+1} + T_{i+1,j-1,k}^{n+1}}{\Delta y^2} + \frac{T_{i+1,j,k+1}^{n+1} - 2T_{i+1,j,k}^{n+1} + T_{i+1,j,k-1}^{n+1}}{\Delta z^2} \right) \\ &- \tilde{\omega}_b C_b \left[\beta T_{i+1,j,k}^{n+1} + (1 - \beta) T_{i+1,j,k}^n \right] + \tilde{Q}_m + \tilde{\omega}_b C_b T_a \end{aligned} \quad (14)$$

$$\begin{aligned}
\tilde{C} \frac{T_{i,j-1,k}^{n+1} - T_{i,j-1,k}^n}{\Delta t} &= \frac{T_{i,j,k}^{n+1} - T_{i,j-1,k}^{n+1}}{S \cdot R_{j-1/2}} + \frac{\tilde{k} (T_{i,j-2,k}^{n+1} - T_{i,j-1,k}^{n+1})}{\Delta y^2} \\
&+ \tilde{k} \left(\frac{T_{i+1,j-1,k}^{n+1} - 2T_{i,j-1,k}^{n+1} + T_{i-1,j-1,k}^{n+1}}{\Delta x^2} + \frac{T_{i,j-1,k+1}^{n+1} - 2T_{i,j-1,k}^{n+1} + T_{i,j-1,k-1}^{n+1}}{\Delta z^2} \right) \\
&- \tilde{\omega}_b C_b \left[\beta T_{i,j-1,k}^{n+1} + (1 - \beta) T_{i,j-1,k}^n \right] + \tilde{Q}_m + \tilde{\omega}_b C_b T_a
\end{aligned} \tag{15}$$

$$\begin{aligned}
\tilde{C} \frac{T_{i,j+1,k}^{n+1} - T_{i,j+1,k}^n}{\Delta t} &= \frac{T_{i,j,k}^{n+1} - T_{i,j+1,k}^{n+1}}{S \cdot R_{j+1/2}} + \frac{\tilde{k} (T_{i,j+2,k}^{n+1} - T_{i,j+1,k}^{n+1})}{\Delta y^2} \\
&+ \tilde{k} \left(\frac{T_{i+1,j+1,k}^{n+1} - 2T_{i,j+1,k}^{n+1} + T_{i-1,j+1,k}^{n+1}}{\Delta x^2} + \frac{T_{i,j+1,k+1}^{n+1} - 2T_{i,j+1,k}^{n+1} + T_{i,j+1,k-1}^{n+1}}{\Delta z^2} \right) \\
&- \tilde{\omega}_b C_b \left[\beta T_{i,j+1,k}^{n+1} + (1 - \beta) T_{i,j+1,k}^n \right] + \tilde{Q}_m + \tilde{\omega}_b C_b T_a
\end{aligned} \tag{16}$$

For the unfrozen and frozen tissue domains, applying the boundary conditions at time $t + \Delta t$ and substituting the calculated results at the previous time t , the unknown T at time $t + \Delta t$ can be solved from Eq. (8). For the blood vessel domain, due to implicit formulations being applied, the unknown T at time $t + \Delta t$ are solved by Gauss-Seidel iteration. After the temperature distributions at time $t + \Delta t$ have been solved, the anterior and posterior moving boundaries can be determined by the isotherms of T_{mu} and T_{ml} , respectively. In order to avoid the numerical instability in Eq. (8), the space and time steps are limited by $1 - W(1 - \beta) \Delta t - m \cdot \text{Fo} \geq 0$. In this study, the grid resolution is $\Delta x = \Delta y = \Delta z = 0.002 \text{ m}$ and $\Delta t = 0.1 \text{ s}$.

The computer code compiled in this article is revised from the code developed in our previous study [46], which had been validated through comparing the numerical results with the exact solution for phase-change problem of a semi-infinite region.

NUMERICAL RESULTS AND DISCUSSION

The tissue domain is prescribed in a rectangular geometry with $10 \text{ cm} \times 10 \text{ cm} \times 20 \text{ cm}$ in the x , y , and z directions respectively, and the dimensions of the tumor, which is located at the center of the tissue region, are $3.2 \text{ cm} \times 3.2 \text{ cm} \times 3.2 \text{ cm}$ for all configurations. The blood flow velocity is set as 10 cm/s , and the vessel diameter is set as 1 mm , based on data from Chato's work [30]. If, in the blood vessel domain, there is one node at which the temperature is below the freezing point of tissue during calculations, the blood flow velocity is set as 0. The constant Nusselt number is taken as $\text{Nu} = 4$ [15, 30]. In the calculations, the cylindrical probe is approximated by a cube. Although the nonuniform grid technique can be introduced to deal with a cylindrical probe surface, this feature is not addressed in this article, for brevity. The probe's acting tip with $16 \text{ mm} \times 8 \text{ mm} \times 8 \text{ mm}$ size is positioned at the domain of $[0.042 \text{ m} \leq x \leq 0.058 \text{ m}, 0.046 \text{ m} \leq y \leq 0.054 \text{ m}, 0.096 \text{ m} \leq z \leq 0.104 \text{ m}]$. The boundary conditions

at the probe surface are prescribed according to the probe tip and probe shank, respectively, as

$$T = T_w \quad \text{at probe tip} \quad (17)$$

$$k \frac{\partial T}{\partial n} = 0 \quad \text{at probe shank} \quad (18)$$

The initial temperature field in tissue is simplified as $T_0(x, y, z) = 37^\circ\text{C}$.

Typical tissue properties are applied as given in [9, 47]: $C_b = C_u = 3.6 \text{ MJ/m}^3 \text{ }^\circ\text{C}$, $C_f = 1.8 \text{ MJ/m}^3 \text{ }^\circ\text{C}$, $k_f = 2 \text{ W/m }^\circ\text{C}$, $k_u = 0.5 \text{ W/m }^\circ\text{C}$, $Q_L = 250 \text{ MJ/m}^3$, $T_a = 37^\circ\text{C}$, $T_{ml} = -8^\circ\text{C}$, $T_{mu} = -1^\circ\text{C}$. The temperature of the probe tip is assumed to be constant ($T_w = -196^\circ\text{C}$). Both the blood perfusion and metabolic rate are very different for normal and tumor tissues [48, 49], and are taken as

$$\omega_b = \begin{cases} 0.0005 \text{ ml/s/ml} & x, y \notin \Omega_t \\ 0.002 \text{ ml/s/ml} & x, y \in \Omega_t \end{cases} \quad (19)$$

$$Q_m = \begin{cases} 4200 \text{ W/m}^3 & x, y \notin \Omega_t \\ 42000 \text{ W/m}^3 & x, y \in \Omega_t \end{cases} \quad (20)$$

respectively, where Ω_t is the tumor domain.

Figures 4 and 5 depict the results for the SATT model, in which the central line of the single artery is at $(x = 0.062 \text{ m}, y = 0.05 \text{ m})$. Figure 4 shows the temperature distribution when $t = 50 \text{ s}$ at cross section $x = 0.062 \text{ m}$, which is at a distance of

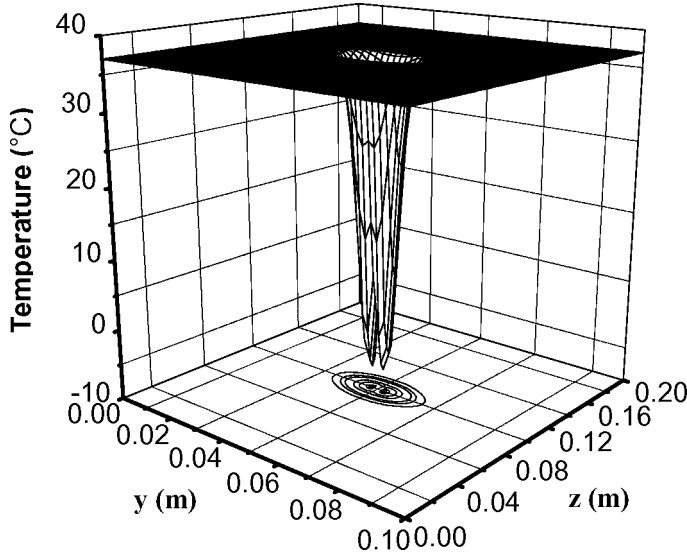


Figure 4. Temperature distribution at cross section $x = 0.062 \text{ m}$ at $t = 50 \text{ s}$ for SATT model.

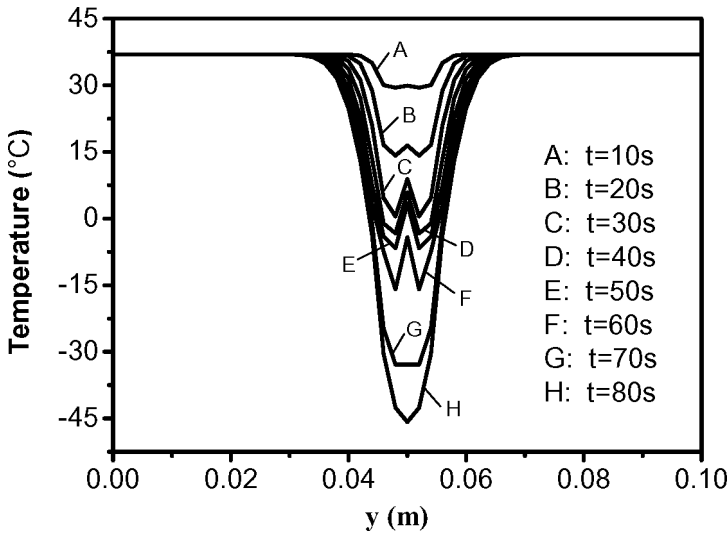


Figure 5. Temperature transients at $x = 0.062$ m, $z = 0.1$ m for SATT model.

4 mm away from the probe tip. Here, as is expected, the temperature distributions of tissues around the probe tip are very different from those of tissues far from the tip. Figure 5 gives the transient temperature distributions at $x = 0.062$ m, $z = 0.1$ m, and curves A–H clearly present the temperature evolutions. In order to better illustrate the effects of blood vessel on the temperature responses of tissue during freezing, similar calculations for the BHTE model have also been performed, and the corresponding results are respectively depicted in Figures 6 and 7 (similarly hereafter for the calculation examples of the SACT and CVCT models). It can be seen from these figures that blood vessels can result in significant difference in temperature responses. Due to the heating behavior of the flowing blood in large blood vessels, the temperature of tissue near the cryoprobe for the case of the SATT model in which a large blood vessel is involved is much higher than that for the case of the BHTE model. This feature is clearly shown in the above figures. It can also be made out from Figure 5 that only after 70 s of freezing is the blood vessel near the cryoprobe already frozen, and thus the circulation of blood vessels is cut off. This may result in bleeding due to rupture of blood vessels by the ice crystal. The loss of blood flow will ultimately result in ischemia and tissue death, so either cutting off circulation of blood vessels or bleeding during the cryoablation procedure may cause undesired damage to healthy tissues or organs. Therefore, it becomes a plague to implement cryosurgery if a critical blood vessel transits the tumor, although blood vessels do seem to tolerate some freezing. Since it is possible to create an iceball immediately adjacent to a vessel wall, the path of the probe also needs to be carefully designed to avoid it being placed too close to major vessels during cryosurgery.

Probe located distant from major vessels is relatively straightforward. Figures 8 and 9 depict the results for the SACT model, in which the central line of the single artery is at $(x = 0.07$ m, $y = 0.05$ m). Figure 8 shows the temperature distribution when $t = 1,200$ s at cross section $x = 0.07$ m, which is at a distance of 12 mm away

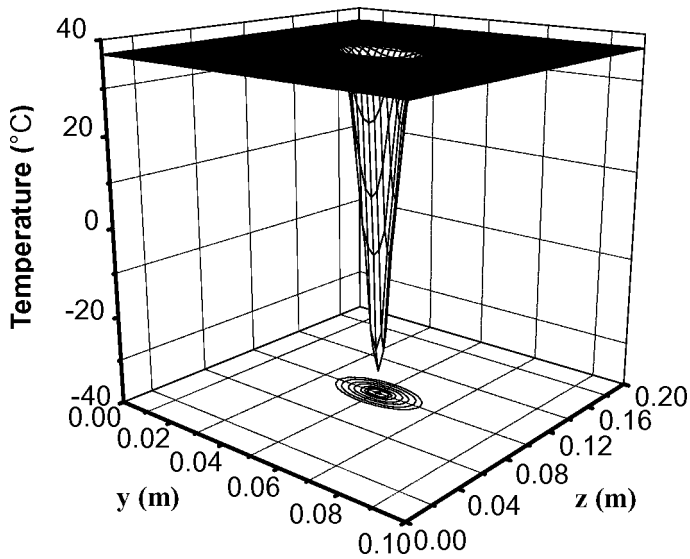


Figure 6. Temperature distribution at cross section $x = 0.062$ m at $t = 50$ s for BHTE model.

from the probe tip. Figure 9 shows the transient temperature distributions at $x = 0.07$ m, $z = 0.1$ m, and curves A–H present the temperature evolutions. The corresponding results for the BHTE model are depicted in Figures 10 and 11, respectively. These figures also indicate that blood vessels can result in evident differences in temperature responses. In addition, the temperature rise near the cryoprobe for the case of the SACT model also presents due to the heating effect of blood flow. From

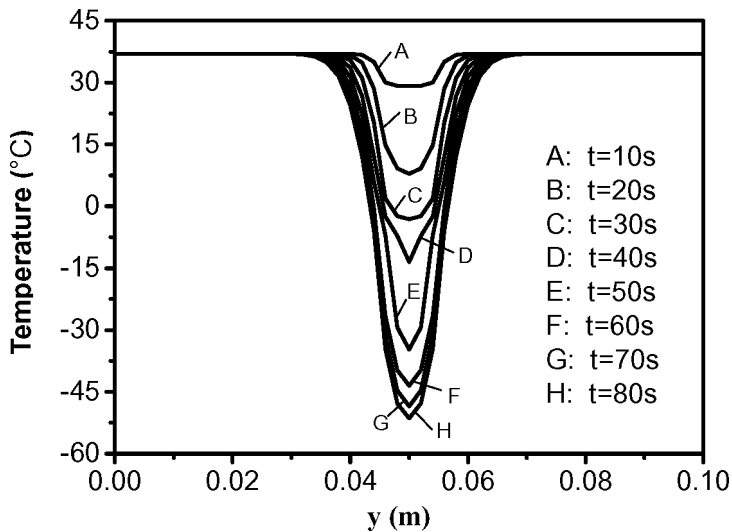


Figure 7. Temperature transients at $x = 0.062$ m, $z = 0.1$ m for BHTE model.

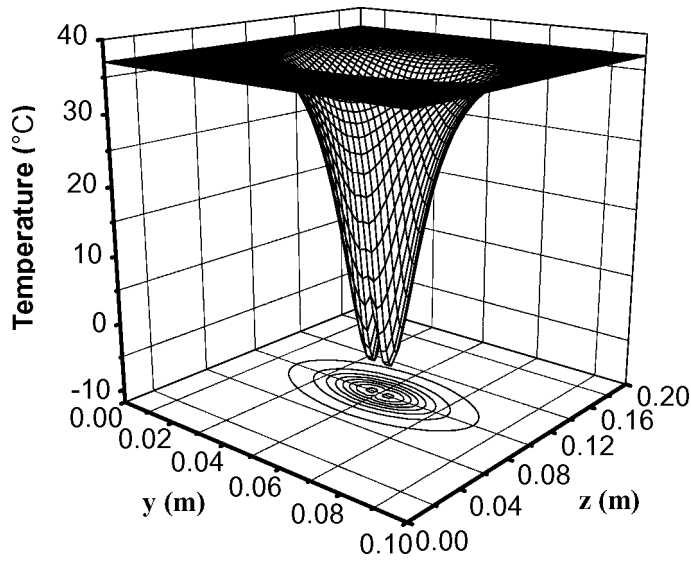


Figure 8. Temperature distribution at cross section $x = 0.07$ m at $t = 1,200$ s for SACT model.

Figure 9, it can be made out that after 1,200 s of freezing, the blood vessel near the cryoprobe has just started to freeze. Generally, such a time is long enough to perform a full freezing process during cryosurgery; meanwhile, the “heat source” effect, created by warm and flowing blood, can prevent damage to the vessel endothelium. This indicates that with appropriate design, an effective cryosurgery for the case of a large blood vessel close to the tumor is possible. However, the heating nature

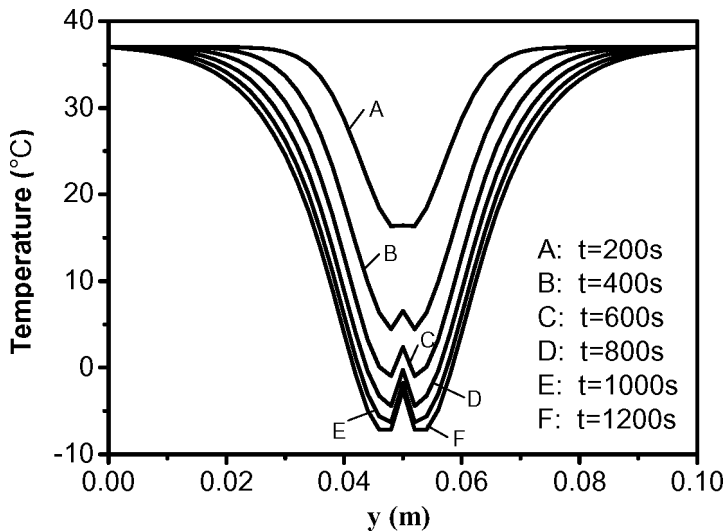


Figure 9. Temperature transients at $x = 0.07$ m, $z = 0.1$ m for SACT model.

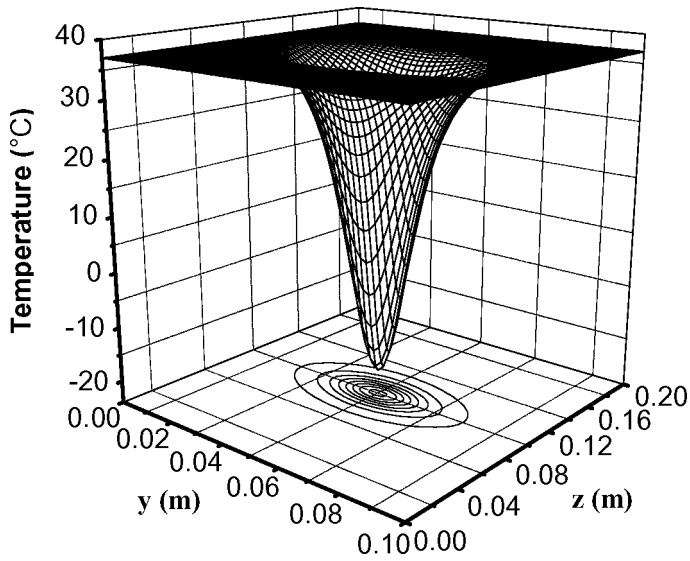


Figure 10. Temperature distribution at cross section $x = 0.07$ m at $t = 1,200$ s for BHTE model.

of blood flow during cryosurgery may also result in inadequate cooling temperatures and then contribute to nonkilling of tumor. Therefore, in order to perform effective cryosurgery when a large blood vessel presents, the effects of large blood vessels on the temperature responses of tissues subject to controlled freezing must be well understood. The numerical results for the CVCT model are depicted in Figures 12 and 13, respectively, in which the central lines of the countercurrent-flow vessels

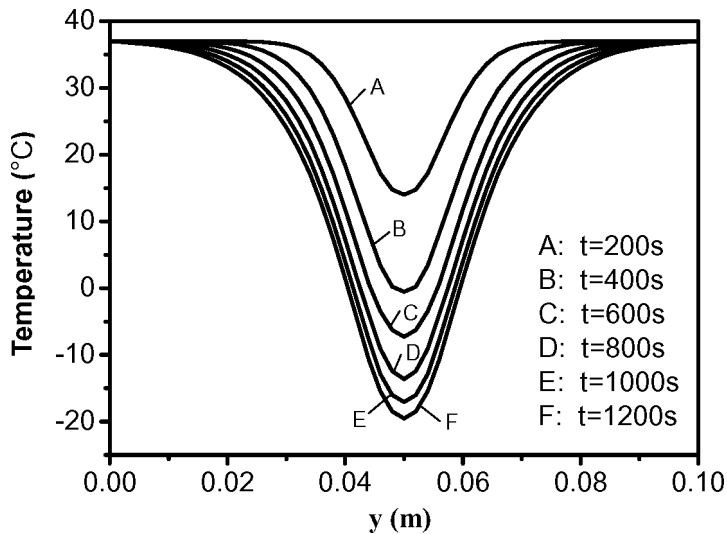


Figure 11. Temperature transients at $x = 0.07$ m, $z = 0.1$ m for BHTE model.

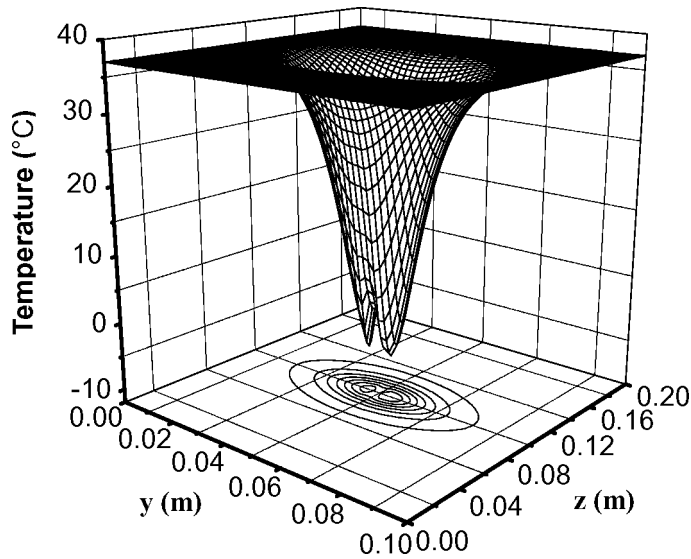


Figure 12. Temperature distribution at cross section $x = 0.07$ m at $t = 1,200$ s for CVCT model.

are at $(x = 0.07$ m, $y = 0.048$ m) and $(x = 0.07$ m, $y = 0.05$ m), respectively. Figure 12 shows the temperature distribution when $t = 1,200$ s at cross section $x = 0.07$ m, and Figure 13 gives the transient temperature distributions at $x = 0.07$ m, $z = 0.1$ m. The results in Figures 12 and 13 further illustrate the effects of large blood vessels on the tissue temperature, and similar conclusions can be made as from the SATT and SACT models. In addition, the nonsymmetrical temperature distribution around

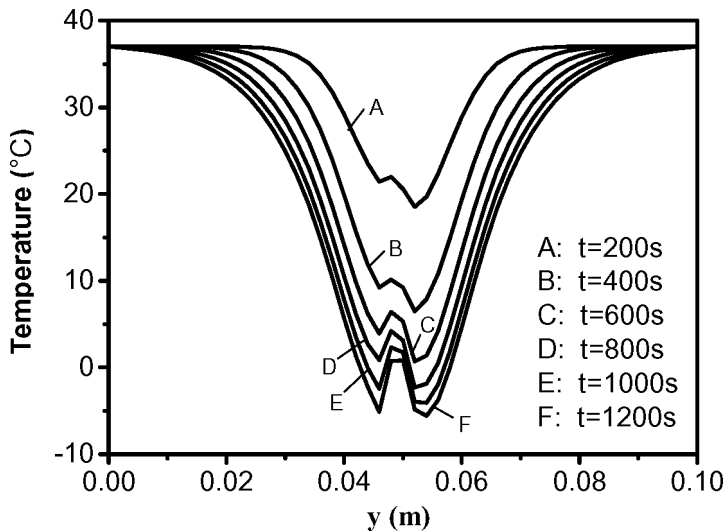


Figure 13. Temperature transients at $x = 0.07$ m, $z = 0.1$ m for CVCT model.

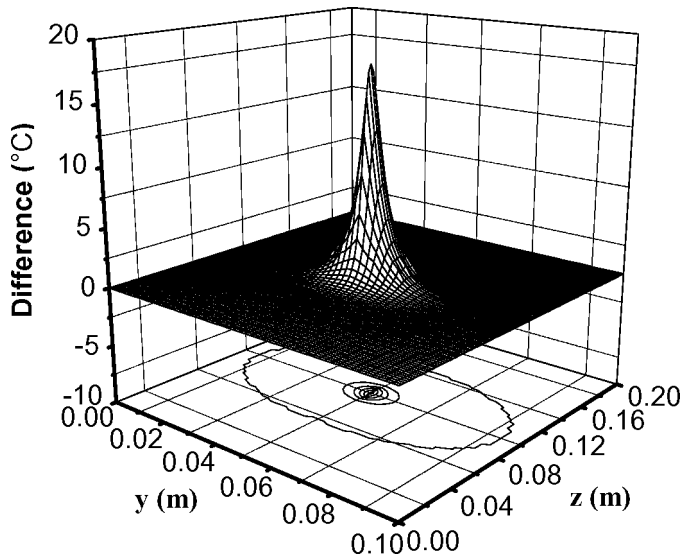


Figure 14. Distribution at cross section $x = 0.066$ m (which is one of the tumor margins) at $t = 1,200$ s for temperature differences between results by SACT model and by BHTE model.

the cryoprobe comes just from the heating of the countercurrent blood flow. Comparisons of the results among all the above models indicate that different vascular models produce significantly different temperature responses for a given freezing pattern.

In order to illustrate the heating effects of large blood vessels quantitatively, the temperature differences between results for the cases of large blood vessel close to the tumor and that for the BHTE model are shown in Figures 14 and 15, respectively. It can be clearly seen that the maximum temperature difference reaches nearly 20°C . So the heating effects of large blood vessels cannot be neglected for a valid treatment planning of cryosurgery.

The location and size of the iceball developed by a particular cryoprobe configuration is important in medical treatment, and its determination will allow the clinician to understand well the freezing necrosis extent as a result of applying a specific probe system. More important, such information is very beneficial for preselecting the correct probe parameters to realize a desirable lesion size. In order to show the effects of large blood vessels on the iceball parameters, the ice fronts at cross section $x = 0.07$ m and $t = 1,200$ s for the CVCT and BHTE models are depicted as examples in Figure 16. It is clearly shown that, due to the heating effects of blood flow, the size of the iceball for the CVCT model is much less than that for the BHTE model. It further indicates that the heating effects of large blood vessels during cryosurgery may result in inadequate freezing and then contribute to incomplete tumor killing.

To eliminate unfrozen regions in tumors and to obtain improved cryosurgery temperature fields, optimal freezing protocols must be found. Since the present study involves three-dimensional inhomogeneous models with different types and

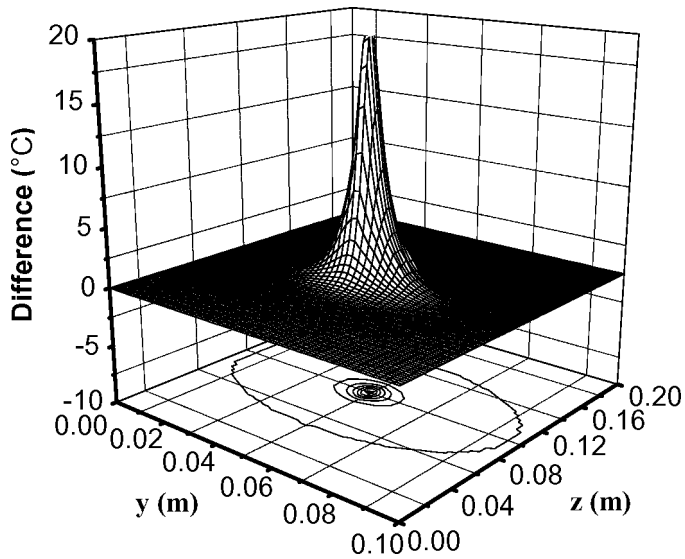


Figure 15. Distribution at cross section $x = 0.066$ m (which is one of the tumor margins) at $t = 1,200$ s for temperature differences between results by CVCT model and by BHTE model.

configurations of blood vessels, a complete optimization study would involve many parameters and be very complicated. Therefore, an exhaustive optimization study is beyond the scope of this work.

Further, multiple cryoprobes can be used to create an iceball that embraces a vessel while not freezing the blood vessel, which potentially necessitates the use of

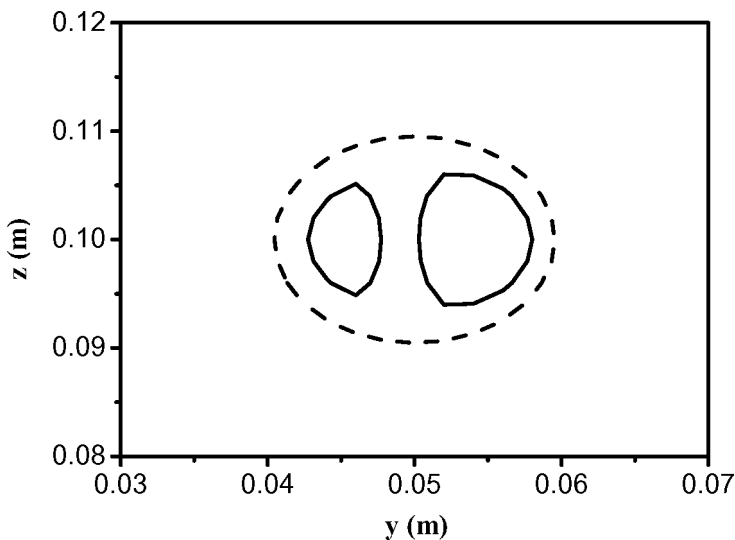


Figure 16. Ice fronts at cross section $x = 0.07$ m and $t = 1,200$ s for BHTE and CVCT models; — represents ice front for CVCT model and - - - - represents ice front for BHTE model.

a treatment system with multiple probes. With the increase in the number of probes, a new challenge is raised. That is, the cryosurgery treatment planning tools or optimization techniques need to be developed. As demonstrated above, the numerical algorithm developed in this article can be applied to solve the complex heat transfer problems with phase change in biological tissues embedded with large blood vessels. With clear knowledge of tissue temperature response to the given conditions, it may be possible to obtain optimal freezing parameters. In addition, in contrast to the freezing process, effects of large blood vessels on the temperature transients during thawing of partially frozen tumors with large blood vessels can be similarly studied by the present method. Moreover, considering that the vessel diameter in this study is limited by the thermal model describing heat transfer to or from large vessels [shown in Eq. (6)], which is based on a heat transfer coefficient derived from analytical solutions of forced convection in cylindrical ducts, detailed parametric analysis of the vessel diameter influence on the aspects of iceball formation and transient temperature profiles has not been presented. These issues are worthy of further investigation.

CONCLUSIONS

This study develops an effective capacity-based numerical algorithm for solving three-dimensional phase-change processes in biological tissues embedded with large blood vessels. In the algorithm, both the convective mechanisms for the directional blood flow in the large vessels and the thermal source effects for the perfused blood, which is used in an attempt to account for the collective heat transfer behaviors of the blood flow in the smaller vessels, are considered. Using this algorithm, the effects of large blood vessels on the tissue temperature distributions during cryosurgery are investigated. The comprehensive computational results indicate that different vascular models produce significantly different temperature patterns, and that the heating effects of large blood vessels during cryosurgery may result in inadequate freezing and then contributing to nonkilling of tumor. This indicates the importance of considering the vasculature for cryosurgery temperature prediction. Based on the present research, the optimal protocol for cryotreating tissues embedded with large blood vessels can perhaps be carried out in future clinical practices.

REFERENCES

1. B. Rubinsky, Cryosurgery, *Annu. Rev. Biomed. Eng.*, vol. 2, pp. 157–187, 2000.
2. D. W. Siemann, Vascular Targeting Agents, *Horizons Cancer Therap.*, vol. 3, no. 2, pp. 4–15, 2002.
3. K. M. Horton and E. K. Fishman, Multidetector CT Angiography of Pancreatic Carcinoma: Part I, Evaluation of Arterial Involvement, *Am. J. Roentgenol.*, vol. 178, pp. 827–831, 2002.
4. Y. T. Zhang, J. Liu, and Y. X. Zhou, Pilot Study on Cryogenic Heat Transfer in Biological Tissues Embedded with Large Blood Vessels, *Forsch. Ing. (Eng. Res.)*, vol. 67, pp. 188–197, 2002.
5. A. P. Ladd, F. J. Rescorla, J. G. Baust, M. Callahan, M. Davis, and J. L. Grosfeld, Cryosurgical Effects on Growing Vessels, *Am. Surgeon*, vol. 65, pp. 677–682, 1999.

6. A. A. Gage, G. Fazekas, and E. E. Riley, Freezing Injury to Large Blood Vessels in Dogs, *Surgery*, vol. 61, pp. 748–754, 1967.
7. N. E. Hoffmann and J. C. Bischof, Cryosurgery of Normal and Tumor Tissue in the Dorsal Skin Flap Chamber: Part I—Thermal Response, *ASME J. Biomech. Eng.*, vol. 123, pp. 301–309, 2001.
8. J. C. Rewcastle and G. A. Sandison, A Model for the Time Dependent Three-Dimensional Thermal Distribution within Iceballs Surrounding Multiple Cryoprobes, *Med. Phys.*, vol. 28, pp. 1125–1137, 2001.
9. Y. Rabin and A. Shitzer, Numerical Solution of the Multidimensional Freezing Problem during Cryosurgery, *ASME J. Biomech. Eng.*, vol. 120, pp. 32–37, 1998.
10. Z. S. Deng and J. Liu, Modeling of Multidimensional Freezing Problem during Cryosurgery by the Dual Reciprocity Boundary Element Method, *Eng. Anal. Bound. Elem.*, vol. 28, pp. 97–108, 2004.
11. Y. T. Zhang and J. Liu, Numerical Study on Three-Region Thawing Problem during Cryosurgical Re-warming, *Med. Eng. Phys.*, vol. 24, pp. 265–277, 2002.
12. R. J. Schweikert and R. G. Keanini, Finite Element and Order of Magnitude Analysis of Cryosurgery in the Lung, *Int. Commun. Heat Mass Transfer*, vol. 26, pp. 1–12, 1999.
13. H. M. Budman, A. Shitzer, and S. Del Giudice, Investigation of Temperature Fields around Embedded Cryoprobes, *ASME J. Biomech. Eng.*, vol. 108, pp. 42–48, 1986.
14. J. C. Bischof, J. Bastacky, and B. Rubinsky, An Analytical Study of Cryosurgery in the Lung, *ASME J. Biomech. Eng.*, vol. 112, pp. 467–472, 1992.
15. H. W. Huang, C. L. Chan, and R. B. Roemer, Analytical Solutions of Pennes Bio-Heat Transfer Equation with a Blood-Vessel, *ASME J. Biomech. Eng.*, vol. 116, pp. 208–212, 1994.
16. R. J. Rawnsley, R. B. Roemer, and A. W. Dutton, The Simulation of Discrete Vessel Effects in Experimental Hyperthermia, *ASME J. Biomech. Eng.*, vol. 116, pp. 256–262, 1994.
17. J. J. W. Lagendijk, M. Schellekens, J. Schipper, and P. M. Vanderlinden, A Three-Dimensional Description of Heating Patterns in Vascularized Tissues during Hyperthermia Treatment, *Phys. Med. Biol.*, vol. 29, pp. 495–507, 1984.
18. J. Baish, P. S. Ayyaswamy, and K. R. Foster, Heat Transport Mechanisms in Vascular Tissues: A Model Comparison, *ASME J. Biomech. Eng.*, vol. 108, pp. 324–331, 1986.
19. C. K. Charny and R. L. Levin, Bioheat Transfer in a Branching Countercurrent Network during Hyperthermia, *ASME J. Biomech. Eng.*, vol. 111, pp. 263–270, 1989.
20. Z. P. Chen and R. B. Roemer, The Effects of Large Blood Vessels on Temperature Distributions during Simulated Hyperthermia, *ASME J. Biomech. Eng.*, vol. 114, pp. 473–481, 1992.
21. J. Crezee and J. J. W. Lagendijk, Temperature Uniformity during Hyperthermia—The Impact of Large Vessels, *Phys. Med. Biol.*, vol. 37, pp. 1321–1337, 1992.
22. M. C. Kolios, M. D. Sherar, and J. W. Hunt, Large Blood-Vessel Cooling in Heated Tissues: A Numerical Study, *Phys. Med. Biol.*, vol. 40, pp. 477–494, 1995.
23. O. I. Craciunescu, T. V. Samulski, J. R. MacFall, and S. T. Clegg, Perturbations in Hyperthermia Temperature Distributions Associated with Counter-current Flow: Numerical Simulations and Empirical Verification, *IEEE Trans. Biomed. Eng.*, vol. 47, pp. 435–443, 2000.
24. T. C. Shih, H. S. Kou, and W. L. Lin, The Impact of Thermally Significant Blood Vessels in Perfused Tumor Tissue on Thermal Dose Distributions during Thermal Therapies, *Int. Commun. Heat Mass Transfer*, vol. 30, pp. 975–985, 2003.
25. H. S. Kou, T. C. Shih, and W. L. Lin, Effect of the Directional Blood Flow on Thermal Dose Distribution during Thermal Therapy: An Application of a Green's Function Based on the Porous Model, *Phys. Med. Biol.*, vol. 48, pp. 1577–1589, 2003.

26. J. J. W. Lagendijk, Hyperthermia Treatment Planning, *Phys. Med. Biol.*, vol. 45, pp. R61–R76, 2000.
27. B. W. Raaymakers, J. Crezee, and J. J. W. Lagendijk, Comparison of Temperature Distributions in Interstitial Hyperthermia: Experiments in Bovine Tongues versus Generic Simulations, *Phys. Med. Biol.*, vol. 43, pp. 1199–1214, 1998.
28. C. H. Blanchard, G. Gutierrez, J. A. White, and R. B. Roemer, Hybrid Finite Element-Finite Difference Method for Thermal Analysis of Blood Vessels, *Int. J. Hyperthermia*, vol. 16, pp. 341–353, 2000.
29. J. A. White, A. W. Dutton, J. A. Schmidt, and R. B. Roemer, An Accurate, Convective Energy Equation Based Automated Meshing Technique for Analysis of Blood Vessels and Tissues, *Int. J. Hyperthermia*, vol. 16, pp. 145–158, 2000.
30. J. C. Chato, Heat Transfer to Blood Vessels, *ASME J. Biomech. Eng.*, vol. 102, pp. 110–118, 1980.
31. S. Weinbaum and L. M. Jiji, A New Simplified Bioheat Equation for the Effect of Blood Flow on Local Average Tissue Temperature, *ASME J. Biomech. Eng.*, vol. 107, pp. 131–139, 1985.
32. L. Zhu, L. X. Xu, Q. H. He, and S. Weinbaum, A New Fundamental Bioheat Equation for Muscle Tissue—Part II: Temperature of SAV Vessels, *ASME J. Biomech. Eng.*, vol. 124, pp. 121–132, 2002.
33. Q. H. He, L. Zhu, and S. Weinbaum, Effect of Blood Flow on Thermal Equilibration and Venous Rewarming, *Ann. Biomed. Eng.*, vol. 31, pp. 659–666, 2003.
34. H. W. Huang, Z. P. Chen, and R. B. Roemer, A Counter Current Vascular Network Model of Heat Transfer in Tissues, *ASME J. Biomech. Eng.*, vol. 118, pp. 120–129, 1996.
35. J. E. I. Hokkanen, Thermal Role of a Blood Vessel Running through a Temperature Gradient, *Ann. N. Y. Acad. Sci.*, vol. 813, pp. 56–62, 1997.
36. R. B. Roemer, Conditions for Equivalency of Countercurrent Vessel Heat Transfer Formulations, *ASME J. Biomech. Eng.*, vol. 121, pp. 514–520, 1999.
37. O. I. Craciunescu and S. T. Clegg, Pulsatile Blood Flow Effects on Temperature Distribution and Heat Transfer in Rigid Vessels, *ASME J. Biomech. Eng.*, vol. 123, pp. 500–505, 2001.
38. R. B. Roemer and A. W. Dutton, A Generic Tissue Convective Energy Balance Equation: Part I—Theory and Derivation, *ASME J. Biomech. Eng.*, vol. 120, pp. 395–404, 1998.
39. G. M. J. Van Leeuwen, A. N. T. J. Kotte, and J. J. W. Lagendijk, A Flexible Algorithm for Construction of 3-D Vessel Networks for Use in Thermal Modeling, *IEEE Trans. Biomed. Eng.*, vol. 45, pp. 596–604, 1998.
40. A. N. T. J. Kotte, G. M. J. Van Leeuwen, and J. J. W. Lagendijk, Modelling the Thermal Impact of a Discrete Vessel Tree, *Phys. Med. Biol.*, vol. 44, pp. 57–74, 1999.
41. O. I. Craciunescu, B. W. Raaymakers, A. N. T. J. Kotte, S. K. Das, T. V. Samulski, and J. J. W. Lagendijk, Discretizing Large Traceable Vessels and Using DE-MRI Perfusion Maps Yields Numerical Temperature Contours That Match the MR Noninvasive Measurements, *Med. Phys.*, vol. 28, pp. 2289–2296, 2001.
42. B. W. Raaymakers, A. N. T. J. Kotte, and J. J. W. Lagendijk, How to Apply a Discrete Vessel Model in Thermal Simulations When Only Incomplete Vessel Data Are Available, *Phys. Med. Biol.*, vol. 45, pp. 3385–3401, 2000.
43. B. W. Raaymakers, J. Crezee, and J. J. W. Lagendijk, Modelling Individual Temperature Profiles from an Isolated Perfused Bovine Tongue, *Phys. Med. Biol.*, vol. 45, pp. 765–780, 2000.
44. G. M. J. Van Leeuwen, A. N. T. J. Kotte, J. DeBree, J. F. VanderKooijk, J. Crezee, and J. J. W. Lagendijk, Accuracy of Geometrical Modelling of Heat Transfer from Tissue to Blood Vessels, *Phys. Med. Biol.*, vol. 42, pp. 1451–1460, 1997.

45. G. M. J. Van Leeuwen, A. N. T. J. Kotte, B. W. Raaymakers, and J. J. W. Lagendijk, Temperature Simulations in Tissue with a Realistic Computer Generated Vessel Network, *Phys. Med. Biol.*, vol. 45, pp. 1035–1049, 2000.
46. Z. S. Deng and J. Liu, Numerical Simulation on 3-D Freezing and Heating Problems for the Combined Cryosurgery and Hyperthermia Therapy, *Numer. Heat Transfer A*, vol. 46, pp. 587–611, 2004.
47. J. C. Chato, Selected Thermophysical Properties of Biological Materials, in A. Shitzer and E. C. Eberhart (eds.), *Heat Transfer in Medicine and Biology*, pp. 413–418, Plenum Press, New York, 1985.
48. J. Liu, L. Zhu, and L. X. Xu, Studies on the Three-Dimensional Temperature Transients in the Canine Prostate during Transurethral Microwave Thermal Therapy, *ASME J. Biomech. Eng.*, vol. 122, pp. 372–379, 2000.
49. Z. S. Deng and J. Liu, Monte Carlo Method to Solve Multidimensional Bioheat Transfer Problem, *Numer. Heat Transfer B*, vol. 42, pp. 543–567, 2002.